Electronic Supplementary Material (ESI) for Journal of Materials Chemistry A.
This journal is © The Royal Society of Chemistry 2024

Supporting Information

N/O coordinated s-Block Potassium Atoms as High-Active Sites for Electroreduction of CO_2 to CO

*Yafei Qu, Peichen Wang, Wei Zheng, Naiyuan Duan, Yang Yang, Tianxin Hou, Chenyang Bi, Dongdong Wang and Qianwang Chen**

Hefei National Research Center for Physical Sciences at the Microscale and Department of Materials Science and Engineering, University of Science and Technology of China, Hefei 230026, China.

*Corresponding author. Email address: cqw@ustc.edu.cn

This file includes:

Experimental section

Materials and methods:

All reagents and chemicals that used in the synthesis of different materials are analytically pure (AR grade). Zinc nitrate hexahydrate ($Zn(NO_3)_3 \cdot 6H_2O$, ≥99.0%), Potassium chloride (KCl, ≥99.5%), Potassium hydrogen carbonate ($KHCO_3$, ≥99.5%), , Methanol (CH_4O, ≥99.5%)and Ethanol (C_2H_6O, ≥99.7%) were purchased from Sinopharm Chemical Reagent Co., Ltd. 2-Methylimidazole ($C_4H_6N_2$ 99%) was purchased from J&K Scientific. Nafion solution (Nafion 1100W, 5 wt.%) was purchased from Sigma-Aldrich. All chemicals were used as received without further purification.

Preparation of catalysts

Synthesis of ZIF-8 precursor: 1.68 g $Zn(NO_3)_2 \cdot 6H_2O$ and 4 g 2-methylimidazole were dissolved in 20 mL and 60 mL methanol, respectively. The two solutions were mixed and stirred for 1 h at room temperature and then left to rest for 24 h. The precipitate was centrifuged and washed with methanol several times and dried at 60℃ under vacuum, denoted as ZIF-8.

Synthesis of K−N, O/C catalysts: A certain mass ratio of ZIF-8 precursors and KCl are mixed intensively in a mortar. Then the mixture is placed in a crucible and pyrolyzed at 900°C under Ar atmosphere for 3 h with a heating rate of 5 °C min^{-1}, the product is labeled as K−N, O/C-pre. K−N, O/C-pre was leached by dilute HCl solution to remove the KCl and remaining Zn. Then, the precipitate was collected and washed with water for several times until its pH was close to 7 and dried in oven at 60 °C. The acid pickling sample was conducted at 900°C under Ar atmosphere for 3 h with a heating rate of 5 °C min^{-1} for a second pyrolysis to obtain the final product, denoted as K−N, O/C-m (m represents the mass ratio of ZIF-8 to KCl). The samples with different ratio are recorded as K−N, O/C-0.5, K−N, O/C-1.0, K−N, O/C-1.5, K−N, O/C-2.0.

Synthesis of N, O/C: As a control sample, ZIF-8 is pyrolyzed at 900°C under Ar atmosphere for 3 h with a heating rate of 5 °C min^{-1} without adding KCl. The obtained carbon material is labelled as N, O/C.

Synthesis of K−O/C: 0.55 g $Zn(CH_3COO)_2 \cdot 2H_2O$ was dispersed in 10 mL aqueous solution to form solution A. 0.525 g of 1,3,5-benzenetricarboxylic acid was added into 70 mL ethanol to form solution B. Then, solutions of A and B were mixed and ultrasound for 20 min at room temperature. The precipitate was centrifuged and washed with water and ethanol several times and dried at 60℃ under vacuum, denoted as ZnBTC. Replace ZIF8 with ZnBTC, the remaining method is the same as K−N, O/C, and the final product is denoted as K-O/C.

Characterizations

SEM images were conducted on a Carl Zeiss Suprs 40 scanning electron microscope (SEM). TEM images were collected from Hitachi H-7650 transmission electron microscope (TEM) using

an accelerating voltage of 200 kV. The powder X-ray diffraction patterns (XRD) of the samples were recorded with an X-ray diffractometer (Japan Rigaku D/MAX-γA) using Cu-Ka radiation (λ=1.54178 Å) with 2θ range of 10°−80°. High-resolution transmission electron microscopy (HRTEM), high-angle annular dark-field scanning transmission electron microscopy (HAADF-STEM) and energy-dispersive spectroscopy (EDS) mapping analyses were executed on a FEI Talos F200X operating at an accelerating voltage of 200 kV. The X-ray photoelectron spectra (XPS) were recorded on a Kratos Axis supra$^+$ spectrometer with an excitation source of monochromatized Al-Ka (hv = 1486.6 eV). The specific surface area was measured with the Brunauer-Emmett-Teller (BET) method using a MicromeriticsTristar II 3020 instrument. Inductively coupled plasma-atomic emission spectrometer (ICP-AES) were conducted with an iCAP 7400 instrument. Raman spectra were obtained using a Horiba LabRAM SoLeil Raman spectrometer. TGA Q5000IR was used for thermogravimetric analysis (TGA) with a heating rate of 5 ℃ min^{-1} in N_2 atmosphere. The Fourier transform infrared (FT-IR) spectra were collected on a Nicolet iS50 FT-IR spectrometer.

Electrochemical measurements

All the CO_2RR electrochemical measurements were conducted at 25 ℃ by an electrochemical workstation (CHI 660E) in a two-compartment batch cell (H-cell) containing 30 mL of 0.5 M $KHCO_3$ solution. A platinum foil and an Ag/AgCl electrode were used as the counter and the reference electrodes, respectively. Typically, 5 mg of catalyst was dispersed in 15 μL Nafion and 485 μL ethanol solution and sonicated for 10 min to form a homogeneous ink. The working electrode was prepared by dropping 50 μL ink onto 1 cm×1 cm carbon paper electrode. Before all the electrochemical CO_2 reduction tests, a flow high-purity CO_2 with a flow rate of 30 sccm (standard cubic centimeter per minute) was purged into the $KHCO_3$ for 30 min (pH = 7.2). During the CO_2RR test, cyclic voltammetry (CV) measurements was performed for twelve circles with scan rate of 100 mV s^{-1} under the potential range from −1.7 V to 0 V. Linear sweep voltammetry (LSV) was conducted with scan rate of 50 mV s^{-1}. Multiple potential step i-t measurements with several selected potential was performed. All potentials were measured against an Ag/AgCl reference electrode and converted to RHE scale according to Nernst equation ($E_{RHE} = E_{Ag/AgCl} + 0.059 \times pH + 0.197$).

Detection and quantification of gas products

The gas produced during the reaction is continuously fed into the gas chromatography (Agilent 7890B) for the analysis of its composition at each potential. The Faradaic efficiency of the gas product was calculated by following equation [1]:

$$Faradaic\ efficiency = \frac{i_x}{i_{total}} = \frac{n_x \times v_{gas} \times c_x \times F}{i_{total} \times V_m}$$

where i_x is the partial current of product x, i_{total} is the total current, n_x represents the number of electrons transferred towards the formation of 1 mol product x, v_{gas} is the CO_2 flow rate (sccm), c_x represents the concentration of product x detected by gas chromatography (ppm), F is the Faraday constant (96,485 C mol^{-1}), and V_m is the unit molar volume, which is 24.5 L mol^{-1} at room temperature (298.15 K).

***In-situ* attenuated total refraction-infrared spectroscopy (ATR-IR)**

ATR-IR was carried out on a Nicolet iS50 FT-IR spectrometer equipped with an MCT detector cooled with liquid nitrogen. The Au-coated Si semi-cylindrical prism (20 mm in diameter) was used as the conductive substrate for catalysts and the IR refection element. The catalysts suspensions were dropped on the Au/Si surface as the working electrode. A Pt-wire and an Ag/AgCl electrode were used as the counter and the reference electrodes, respectively. The electrolyte was 0.5 M $KHCO_3$, which was constantly purged with CO_2 during the experiment. Chronoamperometry was used for CO_2RR test and was accompanied by the spectrum collection. All spectra were recorded on CO_2-saturated 0.5 M $KHCO_3$ by stepwise switching the potential from 0 V to -1.2 V vs. RHE. The spectrum collected at the open circuit voltage is used for the background subtraction.

Density functional theory (DFT) calculations

The DFT calculations were carried out using the *Vienna Ab Initio Simulation* Package (VASP). This code solves the Kohn-Sham equations of density functional theory (DFT) using a plane-wave basis set and the projector augmented wave (PAW) method. The generalized gradient approximation (GGA) of Perdew-Becke-Ernzerhof (PBE) is used for the exchange-correlation functional[2,3]. The kinetic energy cut off is 400 eV for the plane-wave expansion of the electronic wave function, and the convergence criterion of the electronic self-consistent iteration and forces were set to be 10^{-5} eV and 0.01 eV/Å. A Monkhorst-Pack 3×3×1 k-point grid was used for the structural relaxation. The lattice parameters are a= b=25 Å, c=20 Å, α= β=γ=90°.

The overall reaction pathways of CO_2 to CO processes can be described as follows:

$$* + CO_2\,(g) \rightarrow *CO_2 \qquad (1)$$

$$*CO_2 + H^+\,(aq) + e^- \rightarrow *COOH \qquad (2)$$

$$*COOH + H^+\,(aq) + e^- \rightarrow *CO + H_2O\,(l) \qquad (3)$$

$$*CO \rightarrow CO\,(g) + * \qquad (4)$$

The Gibbs free energies were calculated as follows:

$$\Delta G = \Delta H - T\Delta S + \Delta G_{pH} + \Delta G_U = \Delta E + \Delta E_{ZPE} - T\Delta S + \Delta G_{pH} + \Delta G_U$$

$$\Delta G_{pH} = pH \times k_B T \ln 10$$

Where ΔE is the energy difference between products and reactants from DFT calculations. ΔE_{ZPE}

is the difference in zero-point energy. And ΔS is the change in entropy. T is the temperature (298.15 K). $\Delta G_U = -eU$ is the contribution of electrode potential to ΔG. k_B is the Boltzmann constant (1.38×10^{-23} J K^{-1}).

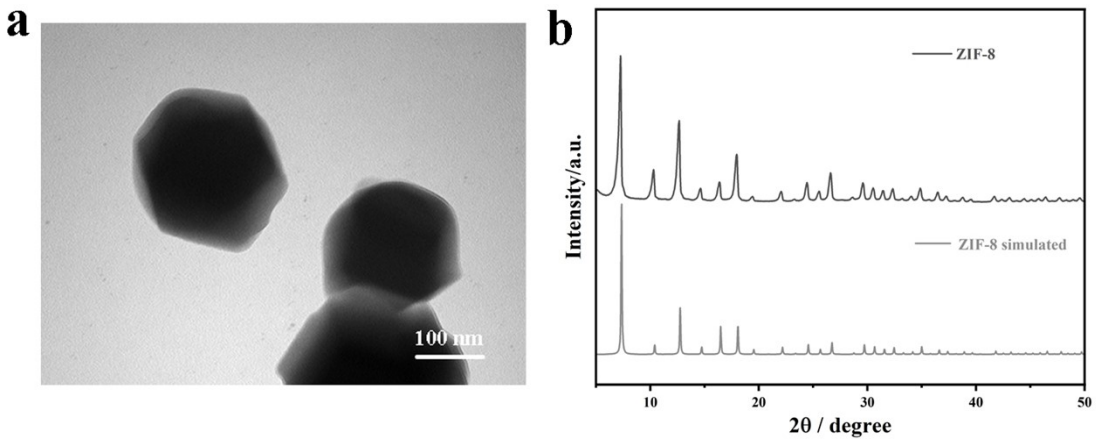

Fig. S1 (a) TEM image of ZIF-8 precursor; (b) The XRD pattern of ZIF-8 precursor.

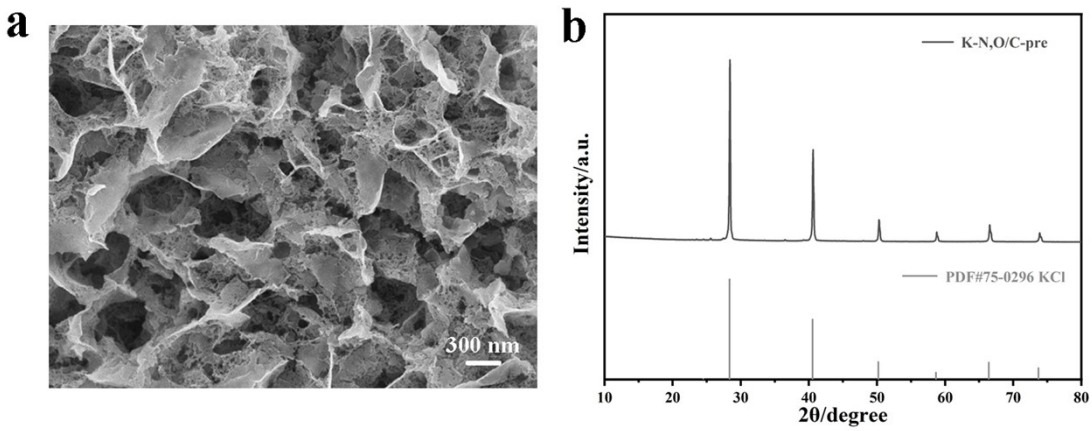

Fig. S2 (a) TEM image of K–N, O/C-pre; (b) The XRD pattern of K–N, O/C-pre.

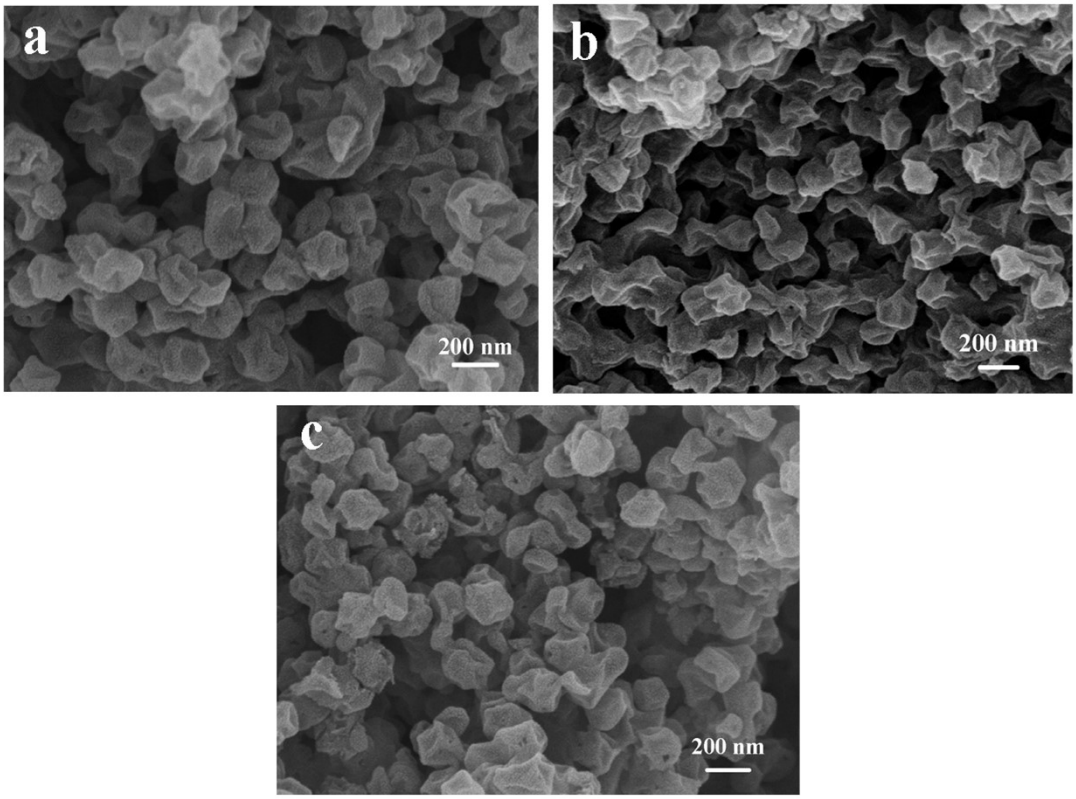

Fig. S3 The SEM images of (a) K–N, O/C-0.5, (b) K–N, O/C-1 and (c) K–N, O/C-2.

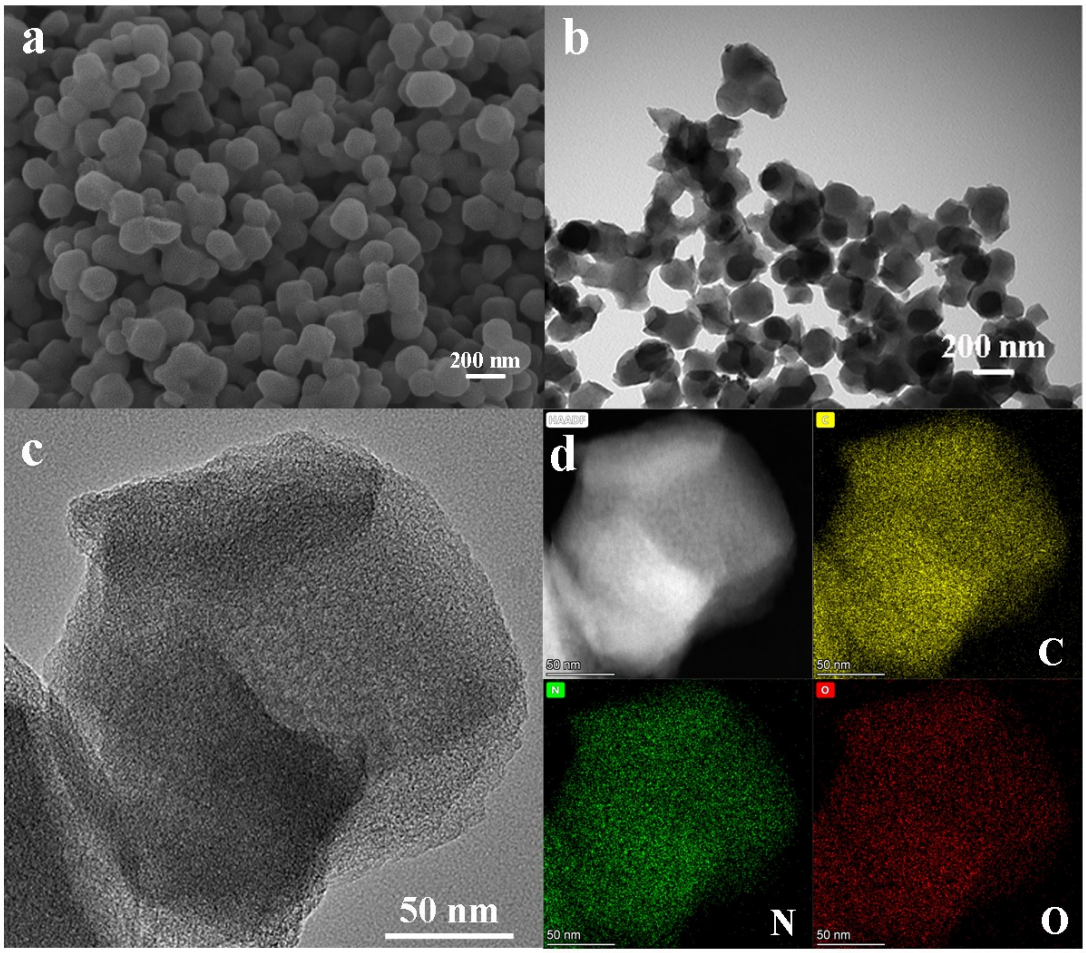

Fig. S4 (a) The SEM images of N, O/C; (b) The TEM images of N, O/C; (c) HRTEM image of N, O/C; (d) HAADF image and elements mapping of N, O/C.

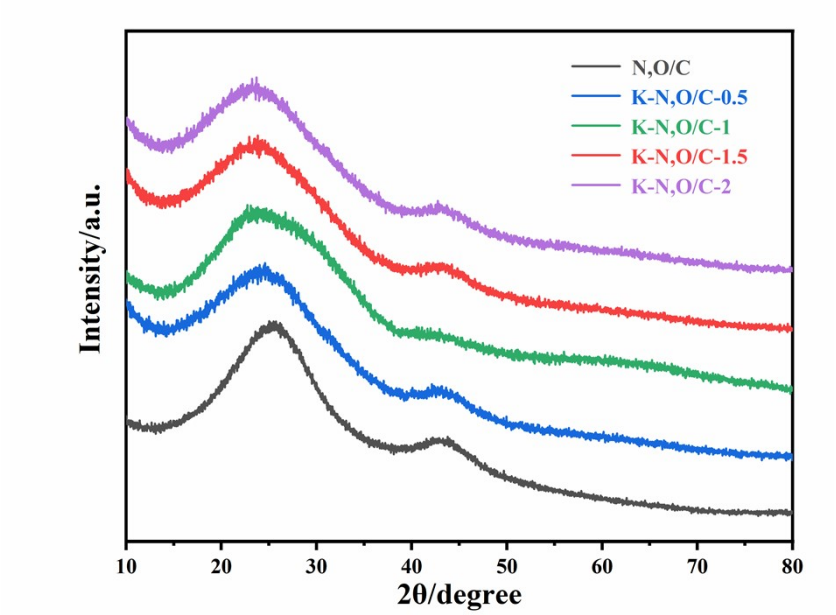

Fig. S5 The XRD patterns of N, O/C, K–N, O/C-0.5, K–N, O/C-1, K–N, O/C-1.5 and K–N, O/C-2.

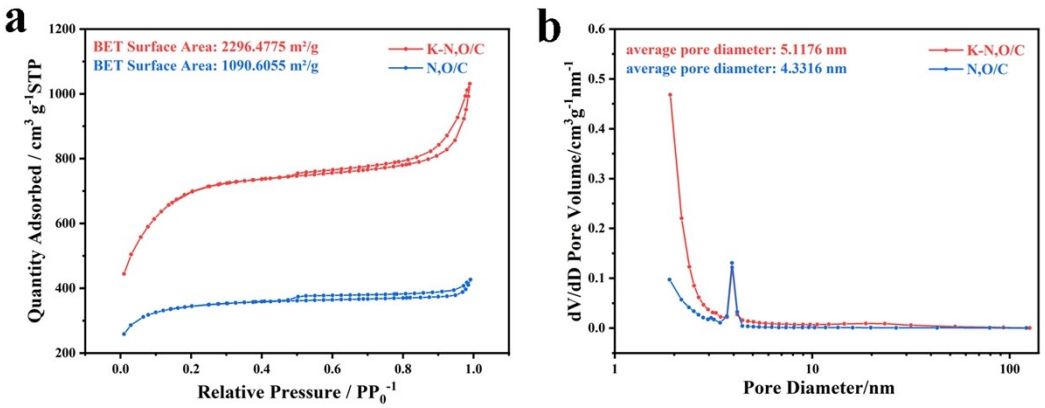

Fig. S6 (a) N_2 adsorption/desorption plots of K–N, O/C and N, O/C catalysts; (b) Pore distribution of K–N, O/C and N, O/C catalysts.

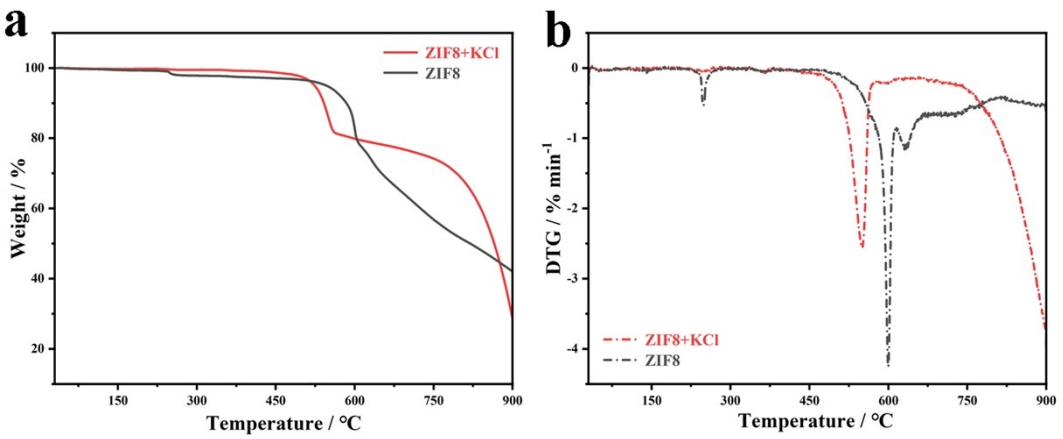

Fig. S7 (a) TG and (b) DTG curves of ZIF-8/KCl under heated from 30 ℃ to 900 ℃ with a rate of 5 ℃ min^{-1} under nitrogen atmosphere.

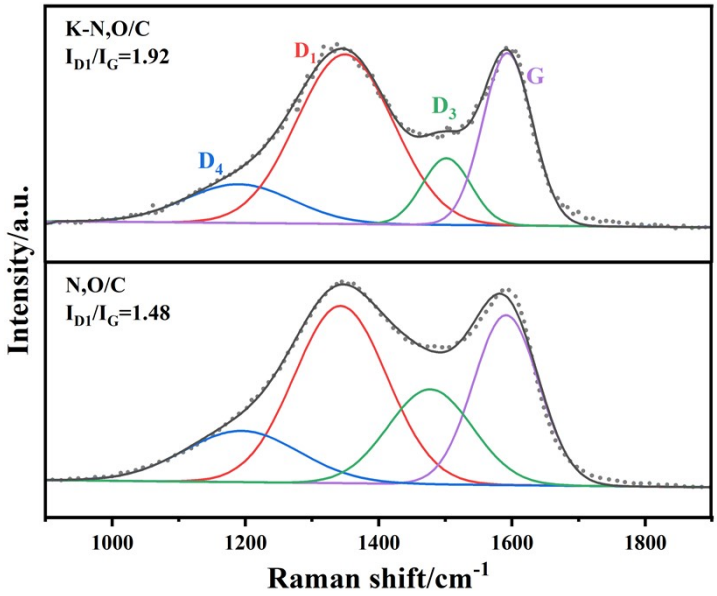

Fig. S8 The Raman spectra of K–N, O/C and N, O/C.

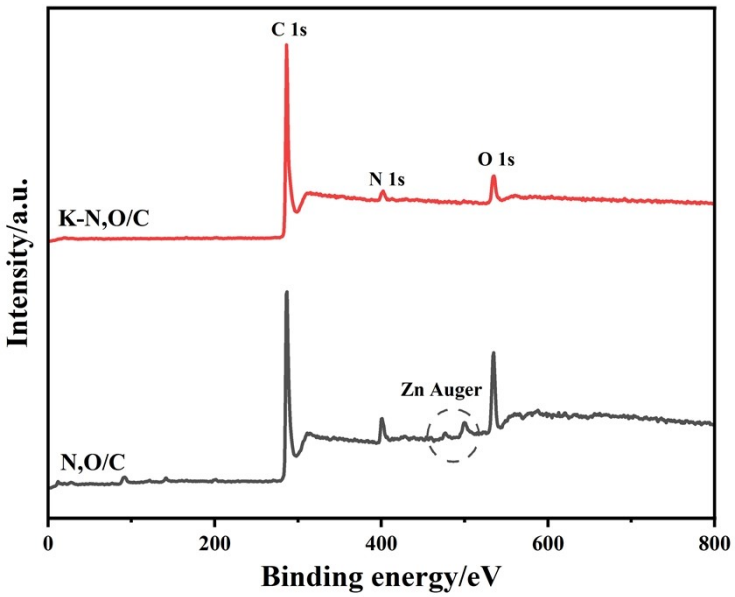

Fig. S9 The XPS survey spectrum of K–N, O/C and N, O/C.

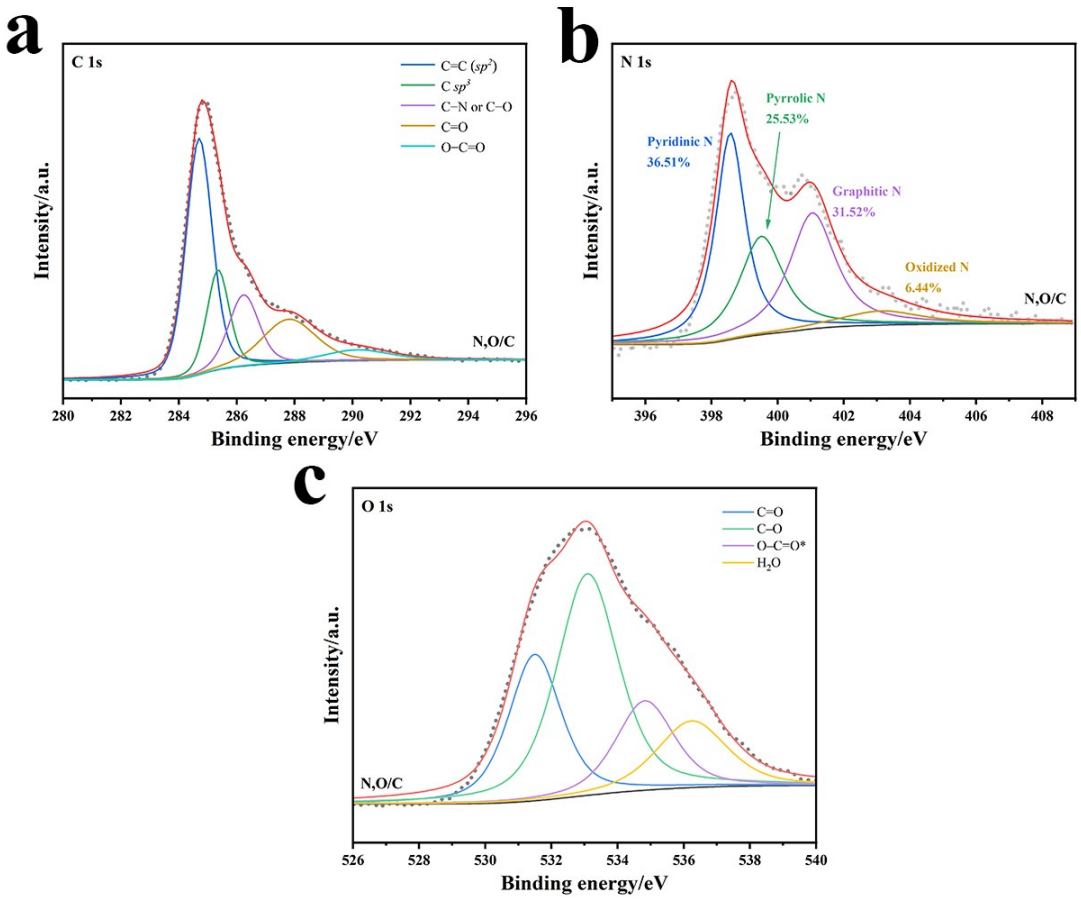

Fig. S10 High-resolution XPS (a) C 1s spectra, (b) N 1s spectra and (c) O 1s spectra of N, O/C.

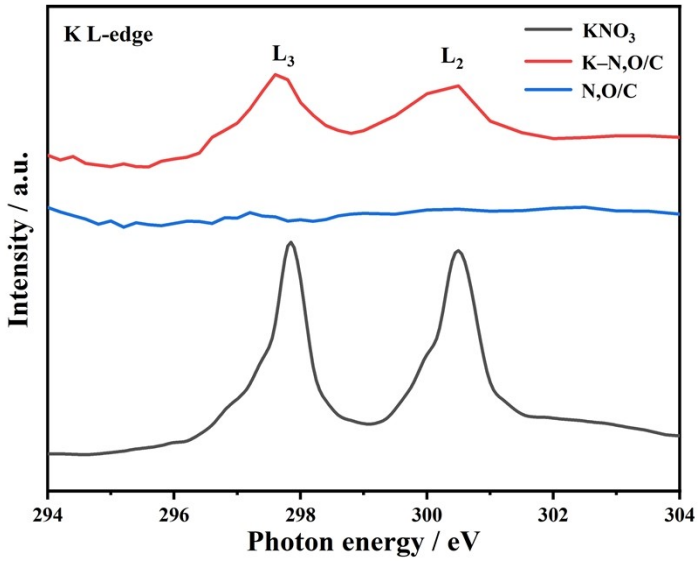

Fig. S11 K L-edge XANES spectra for K–N, O/C and KNO_3.

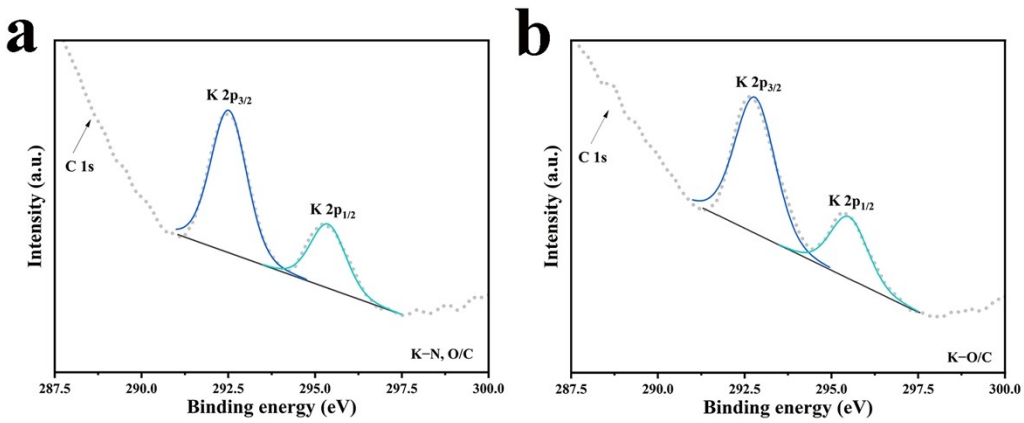

Fig. S12 The high-resolution XPS spectra of K 2p for (a) K–N, O/C and (b) K–O/C.

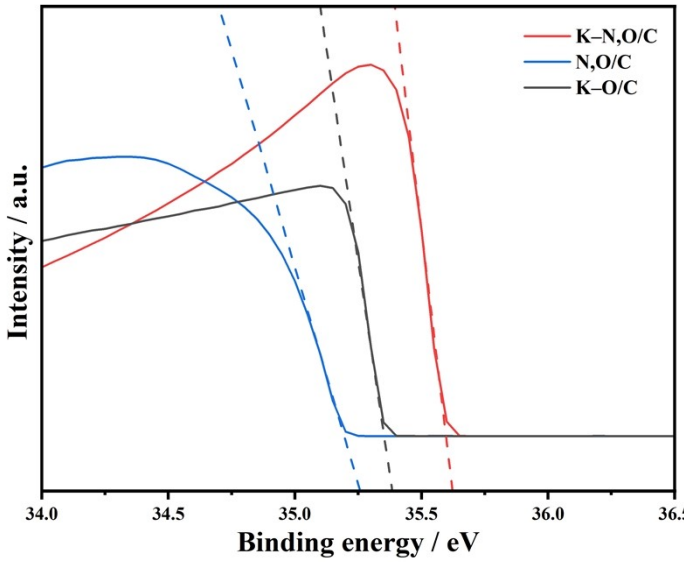

Fig. S13 work function determined by UPS measurements N, O/C, K–O/C and K–N, O/C.

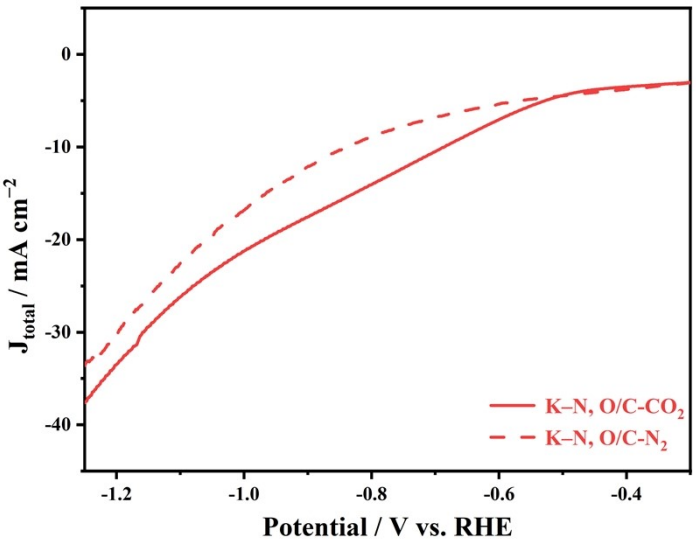

Fig. S14 LSV curves for K–N, O/C in N_2 and CO_2-saturated 0.5 M $KHCO_3$ aqueous solution.

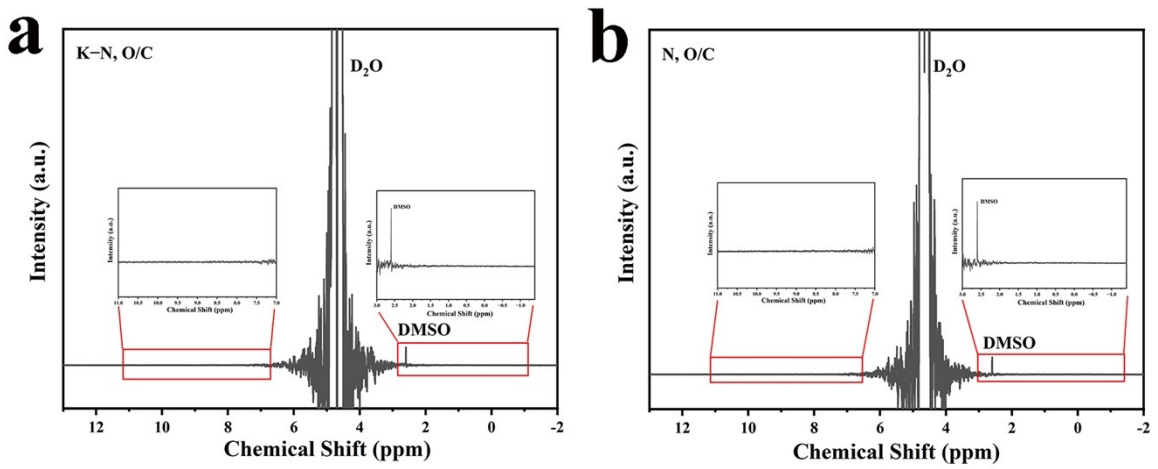

Fig. S15 Liquid products analysis. ^{1}H NMR spectrum of the electrolyte after electrolysis using (a) K–N, O/C and (b) N, O/C at −0.6 V vs. RHE, in which the electrolyte was mixed with of D_2O.

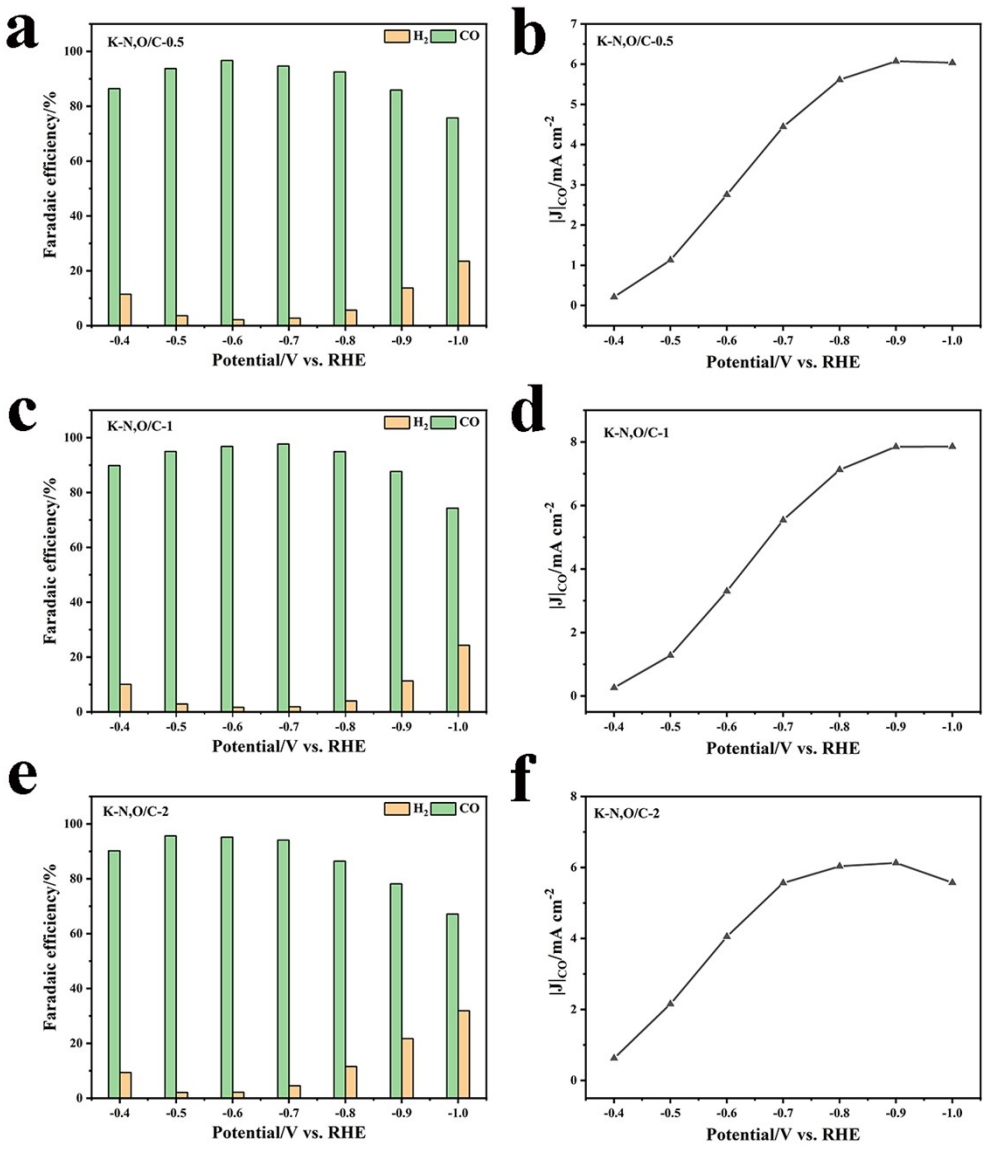

Fig. S16 (a) the FE of H_2 and CO and (b) j_{CO} on K-N, O/C-0.5 in CO_2-saturated 0.5 M $KHCO_3$; (c) the FE of H_2 and CO and (d) j_{CO} on K-N, O/C-1 in CO_2-saturated 0.5 M $KHCO_3$; (e) the FE of H_2 and CO and (f) j_{CO} on K-N, O/C-2 in CO_2-saturated 0.5 M $KHCO_3$.

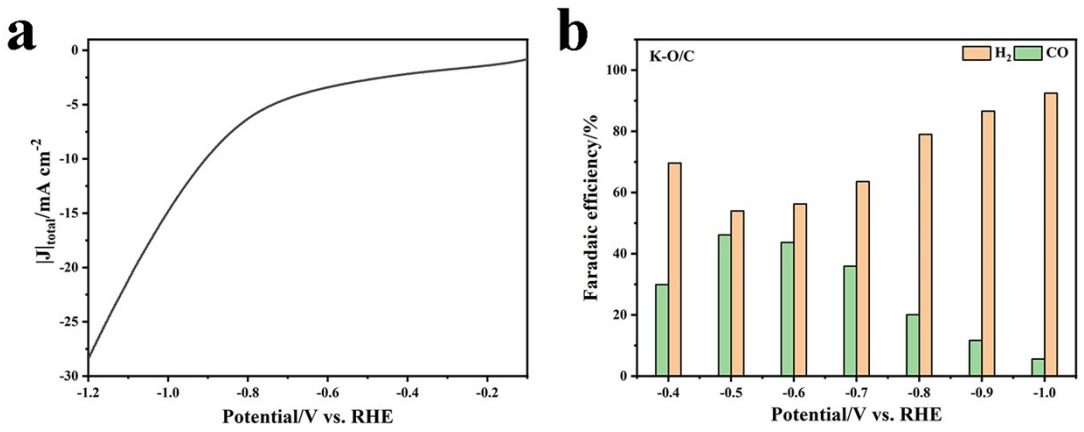

Fig. S17 (a) the total current density (j_{total}) and (b) FE of CO and H_2 on K–O/C in CO_2-saturated 0.5 M $KHCO_3$.

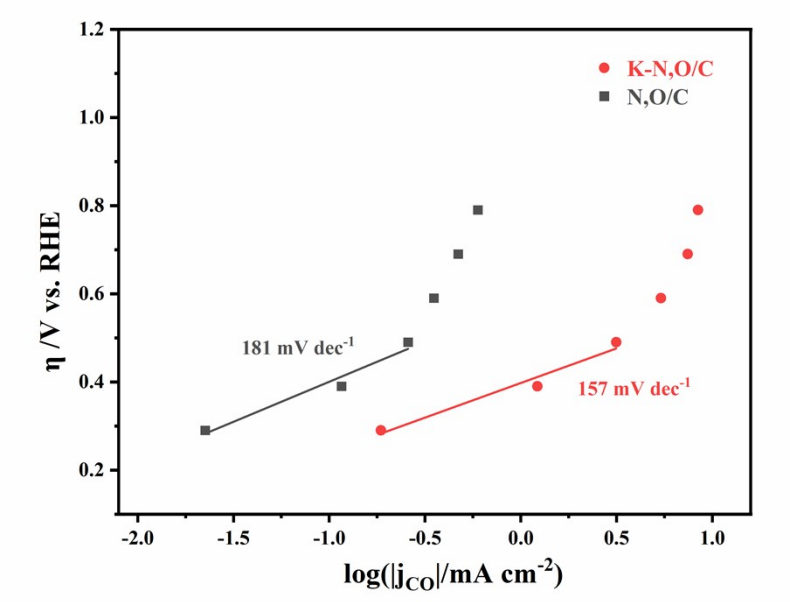

Fig. S18 Tafel slopes of K–N, O/C and N, O/C.

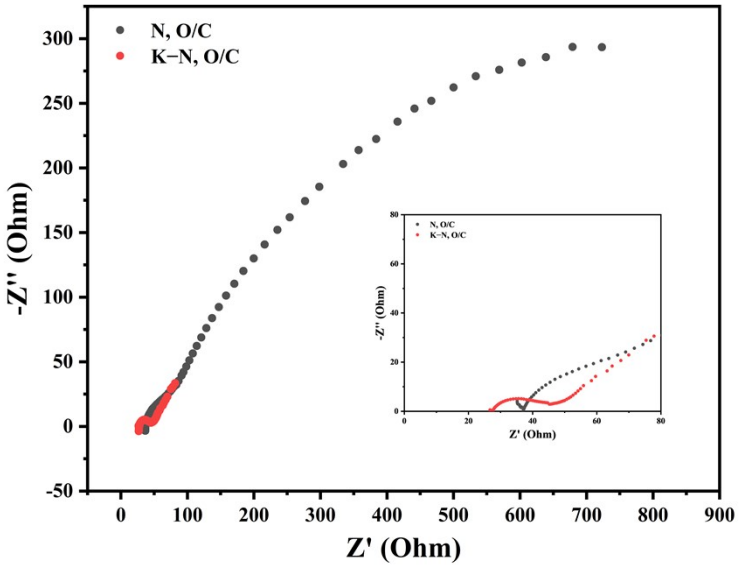

Fig. S19 Nyquist plots of the impedance spectra of K–N, O/C and N, O/C.

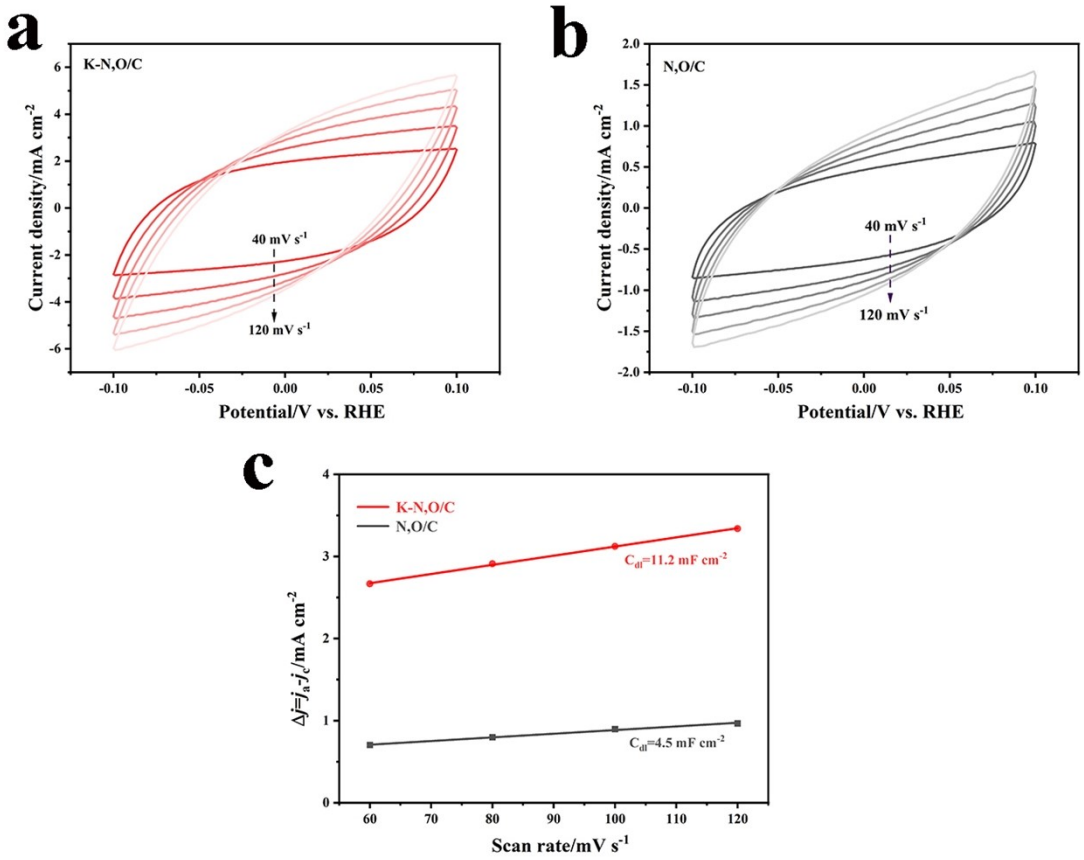

Fig. S20 Electrochemical surface area (ECSA) measurement for different catalysts. CV curves with different scan rates for determining the double-layer capacitance for the (a) K–N, O/C and (b) N, O/C; the calculated C_{dl} values of the (c) K–N, O/C and (d) N, O/C.

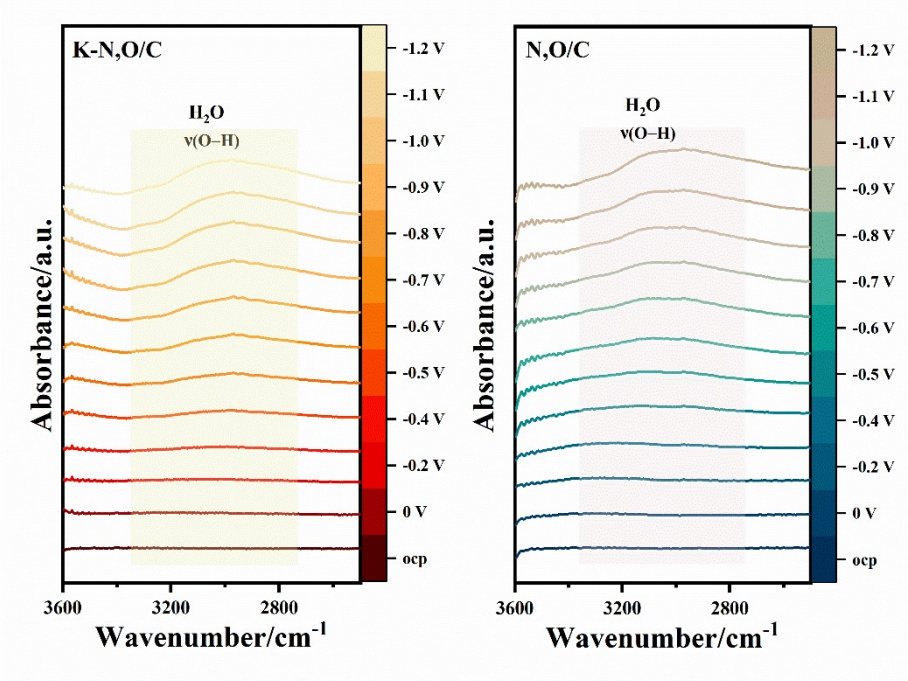

Fig. S21 In situ ATR-FTIR spectra of K–N, O/C and N, O/C in the high wavenumber region recorded at different applied potentials for CO_2RR in CO_2-saturated 0.5 M $KHCO_3$.

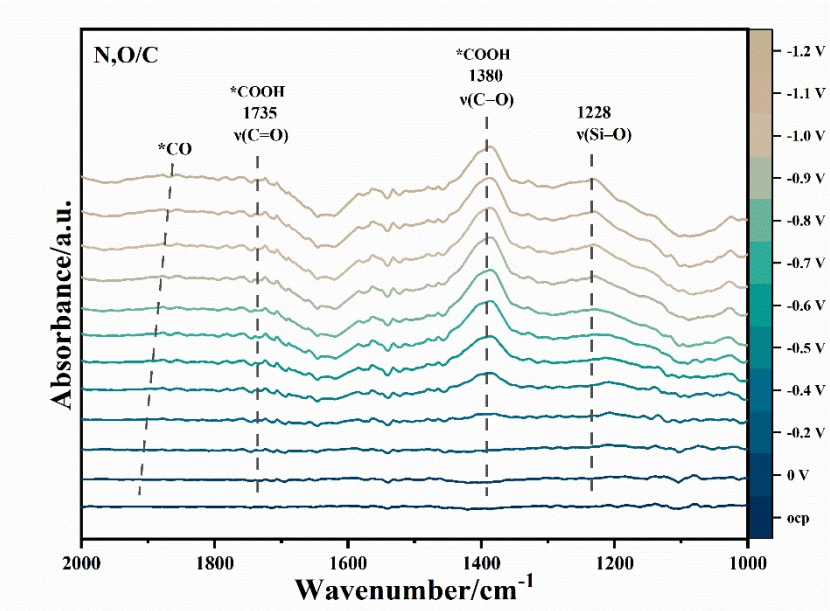

Fig. S22 In situ ATR-FTIR spectra of N, O/C recorded at different applied potentials for CO_2RR in CO_2-saturated 0.5 M $KHCO_3$.

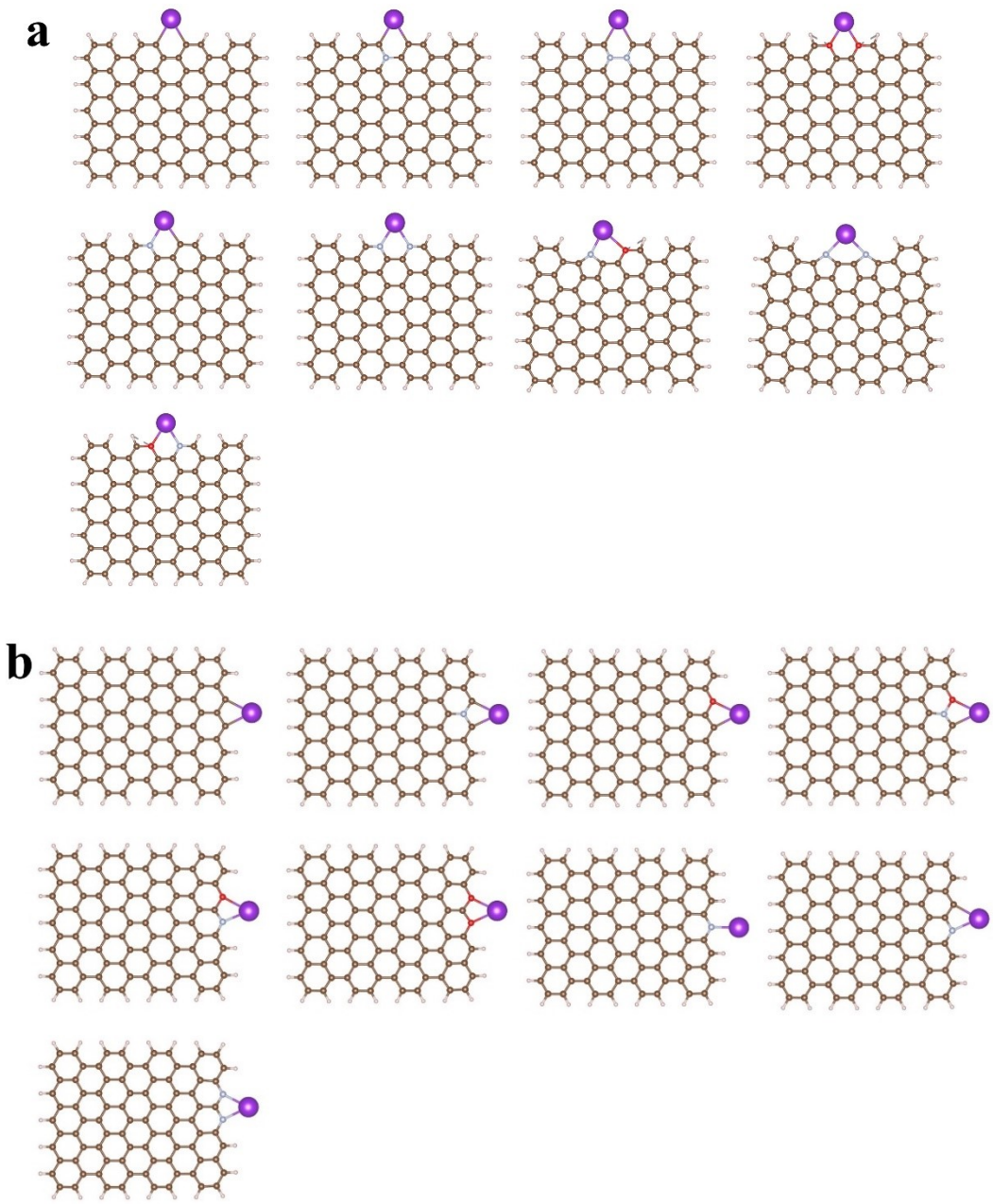

Fig. S23 (a) The optimized structures with armchair-type edge positions, which in order (from left to right, top to bottom) are labelled as the armchair-type K-C2, K-C2-graphitic-N1, K-C2-graphitic-N2, K-O2, K-pyridinic-N1-C1, K-pyridinic-N2, K-pyrrolic-N1-O1 and K-pyrrolic-N2; (b) The optimized structures with zigzag-type edge positions, which in order (from left to right, top to bottom) are labelled as the zigzag-type K-C2, K-C2-graphitic-N1, K-O1-C1, K-O1-graphitic-N1-C1, K-O1-pyridinic-N1, K-O2, K-pyridinic-N1, K-pyridinic-N1-C1 and K-pyridinic-N2. The purple, brown, blue, red and white balls represent K, C, N, O, and H atoms, respectively.

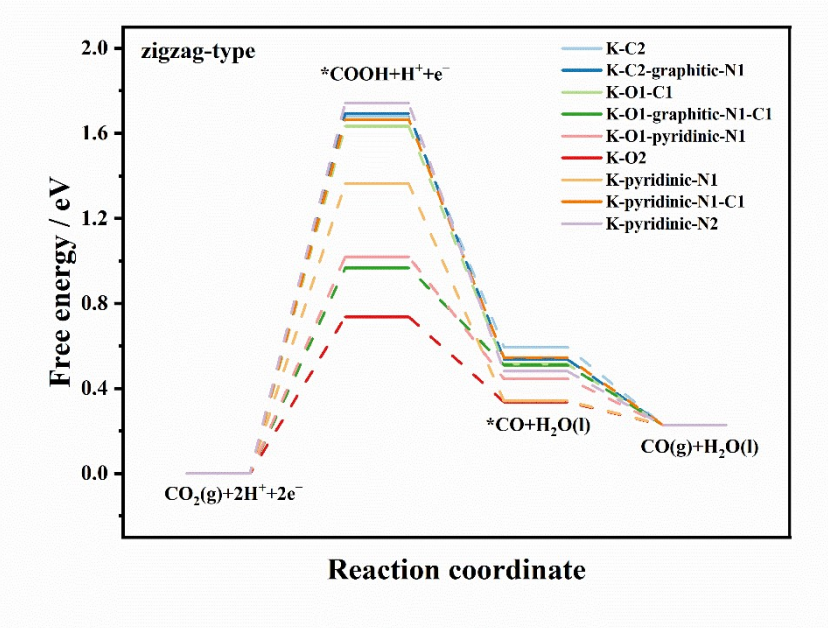

Fig. S24 Gibbs free energy diagrams of CO_2RR on the zigzag-type K embedded in graphene frameworks under U=0V versus RHE.

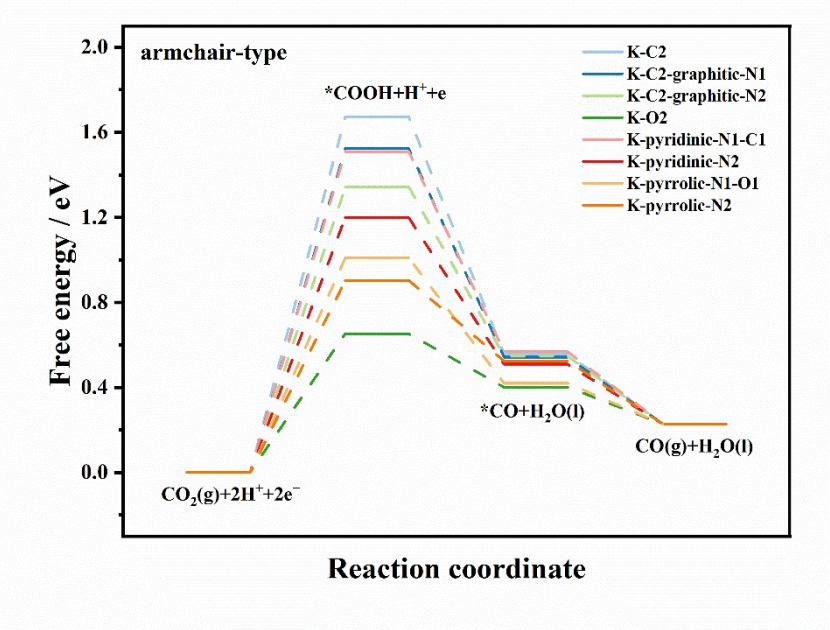

Fig. S25 Gibbs free energy diagrams of CO_2RR on the armchair-type K embedded in graphene frameworks under U=0V versus RHE.

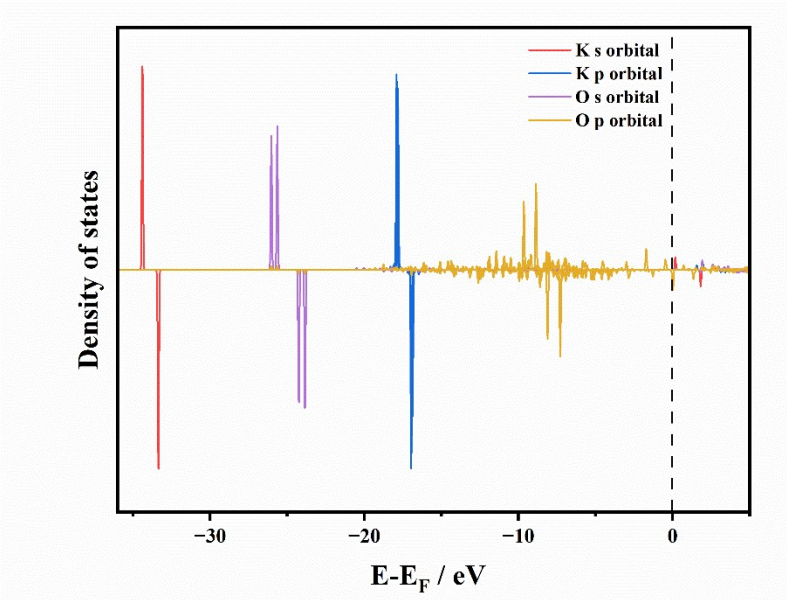

Fig. S26 The PDOS of K and the coordinated O atoms in the armchair-type K-O2.

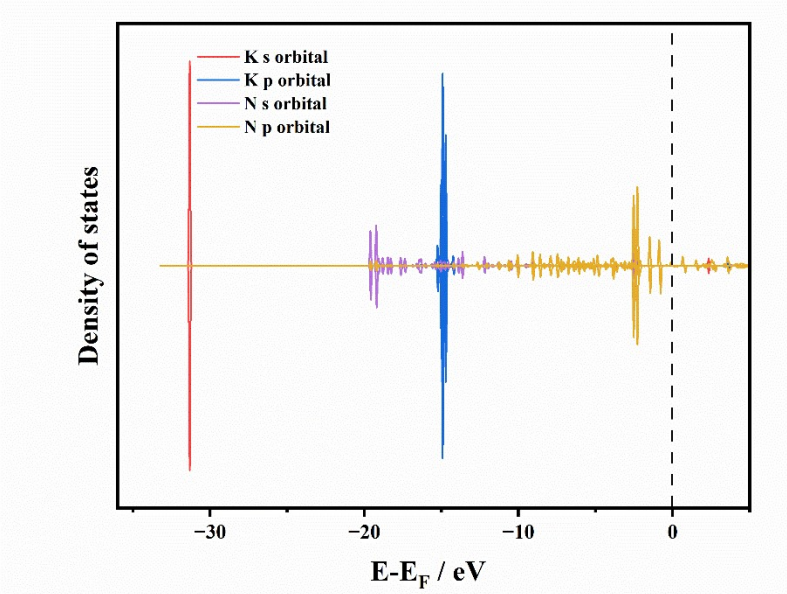

Fig. S27 The PDOS of K and the coordinated N atoms in the armchair-type K-pyrrolic-N2.

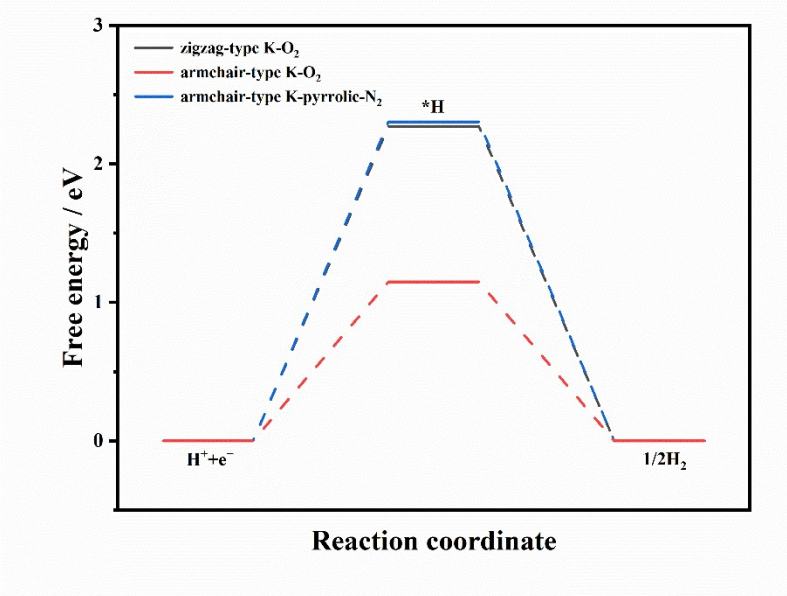

Fig. S28 Gibbs free energy diagrams of HER on the armchair-type K-O2 and zigzag-type K-O2 under U=0V versus RHE.

Table S1. The contents of K and Zn of K–N, O/C and N, O/C obtained from ICP-AES.

Elements (wt. %)	K	Zn
K–N, O/C	0.81	0.3
N, O/C	0.06	9.22

Table S2. Summary of the specific surface area and pore diameter of K–N, O/C and N, O/C.

sample	BET surface area (m^2 /g)	Average pore diameter (nm)
K–N, O/C	2296.48	5.12
N, O/C	1090.61	4.33

Table S3. The contents of C, N, O of K–N, O/C and N, O/C obtained from XPS.

Elements (at. %)	C	N	O
K–N, O/C	90.4	3.4	5.8
N, O/C	80.6	6.0	11.9

Table S4. The reported electrocatalysts for CO_2RR towards CO in H-cell.

Catalysts	Electrolyte ($KHCO_3$)	Potential (V vs. RHE)	FE_{CO} (%)	J_{CO} (mA cm^{-2})	Ref.
K–N, O/C	**0.5**	**−0.6**	**97.8**	**3.15**	**this work**
Li–N, O/C	0.5	−0.5	98.8	2.12	4
Ni-N-C SAC	0.5	−0.65	97	~10	5
Bi-SAs-N/C	0.5 M	−0.7	93.2	4.93	6
FeN4Cl/NC	0.5 M	−0.6	90.5	10.8	7
DPC-NH_3-950	0.1 M	−0.6	95.2	2.84	8
Sn-NOC	0.1 M	−0.7	94	13.9	9
Fe-N-P-C	0.5 M	−0.34	98	0.8	10
CuN_3O/C	0.5 M	−0.8	96	1.8	11
Zn–NS–C	0.5 M	−0.5	96	5.2	12
CNS-NiSA	0.5 M	−0.8	95	7.8	13

REFERENCES

1 M. Huang, S. Gong, C. Wang, Y. Yang, P. Jiang, P. Wang, L. Hu and Q. Chen, *Angew. Chem. Int. Ed.*, 2021, **60**, 23002–23009.

2 G. Kresse and J. Hafner, *Phys. Rev. B*, 1993, **47**, 558–561.

3 P. E. Blöchl, *Phys. Rev. B*, 1994, **50**, 17953–17979.

4 H. Huang, S. Chen, P. Jiang, Y. Yang, C. Wang, W. Zheng, Z. Cheng, M. Huang, L. Hu and Q. Chen, *Adv. Funct. Mater.*, 2023, **33**, 2300475.

5 J. Wang, Y.-C. Huang, Y. Wang, H. Deng, Y. Shi, D. Wei, M. Li, C.-L. Dong, H. Jin, S. S. Mao and S. Shen, *ACS Catal.*, 2023, **13**, 2374–2385.

6 Z. Wang, C. Wang, Y. Hu, S. Yang, J. Yang, W. Chen, H. Zhou, F. Zhou, L. Wang, J. Du, Y. Li and Y. Wu, *Nano Res.*, 2021, **14**, 2790–2796.

7 Z. Li, R. Wu, S. Xiao, Y. Yang, L. Lai, J. S. Chen and Y. Chen, *Chem. Eng. J.*, 2022, **430**, 132882.

8 Y. Dong, Q. Zhang, Z. Tian, B. Li, W. Yan, S. Wang, K. Jiang, J. Su, C. W. Oloman, E. L. Gyenge, R. Ge, Z. Lu, X. Ji and L. Chen, *Adv. Mater.*, 2020, **32**, 2001300.

9 J. Guo, W. Zhang, L. Zhang, D. Chen, J. Zhan, X. Wang, N. R. Shiju and F. Yu, *Adv. Sci.*, 2021, **8**, 2102884.

10 K. Li, S. Zhang, X. Zhang, S. Liu, H. Jiang, T. Jiang, C. Shen, Y. Yu and W. Chen, *Nano Lett.*, 2022, **22**, 1557–1565.

11 P. Song, B. Hu, D. Zhao, J. Fu, X. Su, W. Feng, K. Yu, S. Liu, J. Zhang and C. Chen, *ACS Nano*, 2023, **17**, 4619–4628.

12 W. Zheng, D. Wang, W. Cui, X. Sang, X. Qin, Z. Zhao, Z. Li, B. Yang, M. Zhong, L. Lei, Q. Zheng, S. Yao, G. Wu and Y. Hou, *Energy Environ. Sci.*, 2023, **16**, 1007–1015.

13 X. Zhao, S. Huang, Z. Chen, C. Lu, S. Han, C. Ke, J. Zhu, J. Zhang, D. Tranca and X. Zhuang, *Carbon*, 2021, **178**, 488–496.